Physica A 463 (2016) 37–44

Contents lists available at ScienceDirect

Physica A

journal homepage: www.elsevier.com/locate/physa

Squared sine logistic map

R. Egydio de Carvalho [a,*], Edson D. Leonel [b]

[a] Universidade Estadual Paulista-UNESP, Rio Claro-SP, Brazil

[b] Departamento de Física, UNESP - Univ. Estadual Paulista, Av.24A, 1515 - Bela Vista – 13506-900, Rio Claro-SP, Brazil

HIGHLIGHTS

- We propose a perturbated logistic map.
- We observe different routes to chaos.
- We observe an unlimited sequence of center-saddle bifurcations.
- The Lyapunov diagrams present qualitative differences for the routes to chaos.
- The bifurcations present robust scaling features.

ARTICLE INFO

Article history:
Received 4 July 2016
Available online 15 July 2016

Keywords:
Multi-stability
Bifurcation
Attractor
Perturbed logistic map

ABSTRACT

A periodic time perturbation is introduced in the logistic map as an attempt to investigate new scenarios of bifurcations and new mechanisms toward the chaos. With a squared sine perturbation we observe that a point attractor reaches the chaotic attractor without following a cascade of bifurcations. One fixed point of the system presents a new scenario of bifurcations through an infinite sequence of alternating changes of stability. At the bifurcations, the perturbation does not modify the scaling features observed in the convergence toward the stationary state.

1. Introduction

The logistic map is possibly the most studied one-dimensional map since it is very simple and produces fundamental results on non-linear dynamics [1]. The map allows one to understand the concepts of bifurcations [2], crisis [3,4], route to chaos [5], among other concepts [6–10]. The map is essentially a quadratic function of the type, $f(x_n) = x_{n+1} = rx_n(1 - x_n)$ where r is a control parameter and the map iterations are mapped on the limited range $x \in [0, 1]$ while $r \leq 4$. From this value a boundary crisis occurs [3,4], the chaotic attractive set is destroyed and the iterations escape from this range and go to infinity. There are two fixed points, x^*, for this map, one at $x_1^* = 0$ and another r-dependent given by $x_2^* = (1 - 1/r)$. A transcritical bifurcation is observed at $r = 1$, where the fixed points x_1^* and x_2^* exchange their stability. For $r > 1$, the fixed point x_1^* becomes unstable. For $r = 3$ a first period doubling bifurcation happens involving x_2^*, which defines a route of flip bifurcations, known as Feigenbaum scenario [8,9], toward a chaotic dynamics. For $r = 4$, the fixed point x_1^* touches the chaotic attractor at $x = 0$, producing a boundary crisis, hence destroying the attractor. After the destruction, the chaotic attractor is replaced by a chaotic transient which is characterized by a power law [11]. In order to search for new bifurcations or new mechanisms to chaos, we perturb the logistic map with a squared-sine perturbation. In Section 2 we present our model and the numerical results, including plots of the bifurcation diagram, the associated Lyapunov exponents

* Corresponding author.
E-mail addresses: regydio@rc.unesp.br (R.E. de Carvalho), edleonel@rc.unesp.br (E.D. Leonel).

http://dx.doi.org/10.1016/j.physa.2016.07.008

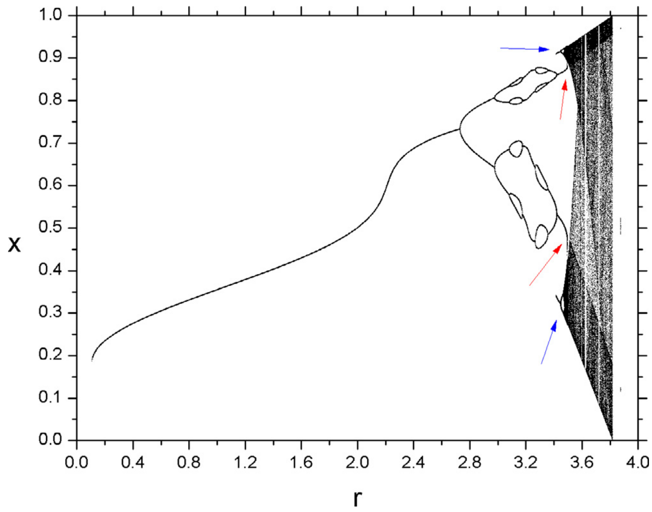

Fig. 1. Bifurcations diagram for the squared sine logistic map. The blue arrows indicate the period doubling cascade toward the chaos, while the red arrows indicate another route to chaos.

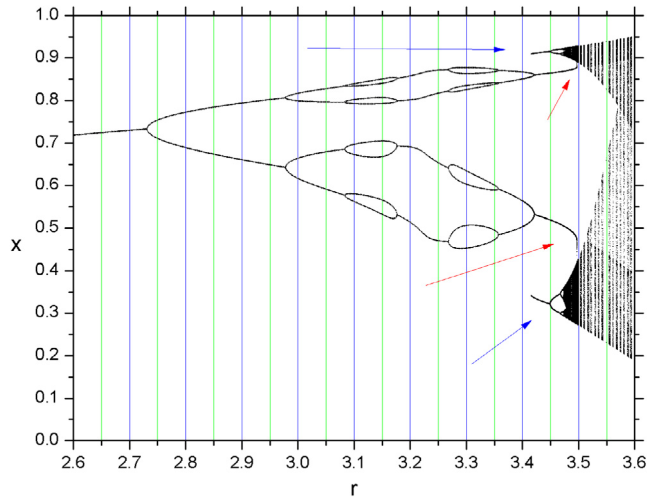

Fig. 2. Amplification of Fig. 1 emphasizing the recomposition regions and the different routes to chaos. The red and blue arrows are to guide the eyes.

and projections of the Lyapunov exponents on the space of the parameters. In Section 3 we present some final remarks and our conclusions. For interpretation of the references to color in the figures legend, the reader is referred to the web version of this article.

2. The model and results

The perturbed map is called as *squared sine logistic map* and it is given through the following mapping,

$$f(x_n) = x_{n+1} = rx_n(1 - x_n) + \mu \sin^2(2\pi x_n). \tag{1}$$

The square used in the periodic function ensures that the iterations remain in the interval $x \in [0, 1]$, when started with positive values of x, and μ is a second control parameter that alters the pattern of the original map and controls the intensity of the sinusoidal non-linear function. It is immediate to see that the value $x = 0$ is always a fixed point. However, the r-dependent fixed point of the logistic map can no longer be obtained analytically. After trying some values for μ, we kept it fixed in 0.2, even though any other value could be considered, and we have obtained the following results.

In Fig. 1, we vary r in [0, 4]. For each value of r we gave some initial values for x in order to search for possibly the coexistence of different attractors. Fig. 2 is an amplification of Fig. 1 in the range $r \in [2.6, 3.6]$. We observed that around $r \sim 2.73$, the second fixed point experiences a flip bifurcation, which bifurcates again for $r \sim 2.97$ and $r \sim 3.09$. In the range $r \in [3.09, 3.18]$ there is an attractor with period-8, however differently of the very well-known bifurcation cascade, for $r \sim 3.18$ occurs a recomposition of the attractor reducing its period to 4. From $r \sim 3.27$ up to $r \sim 3.36$ the attractor

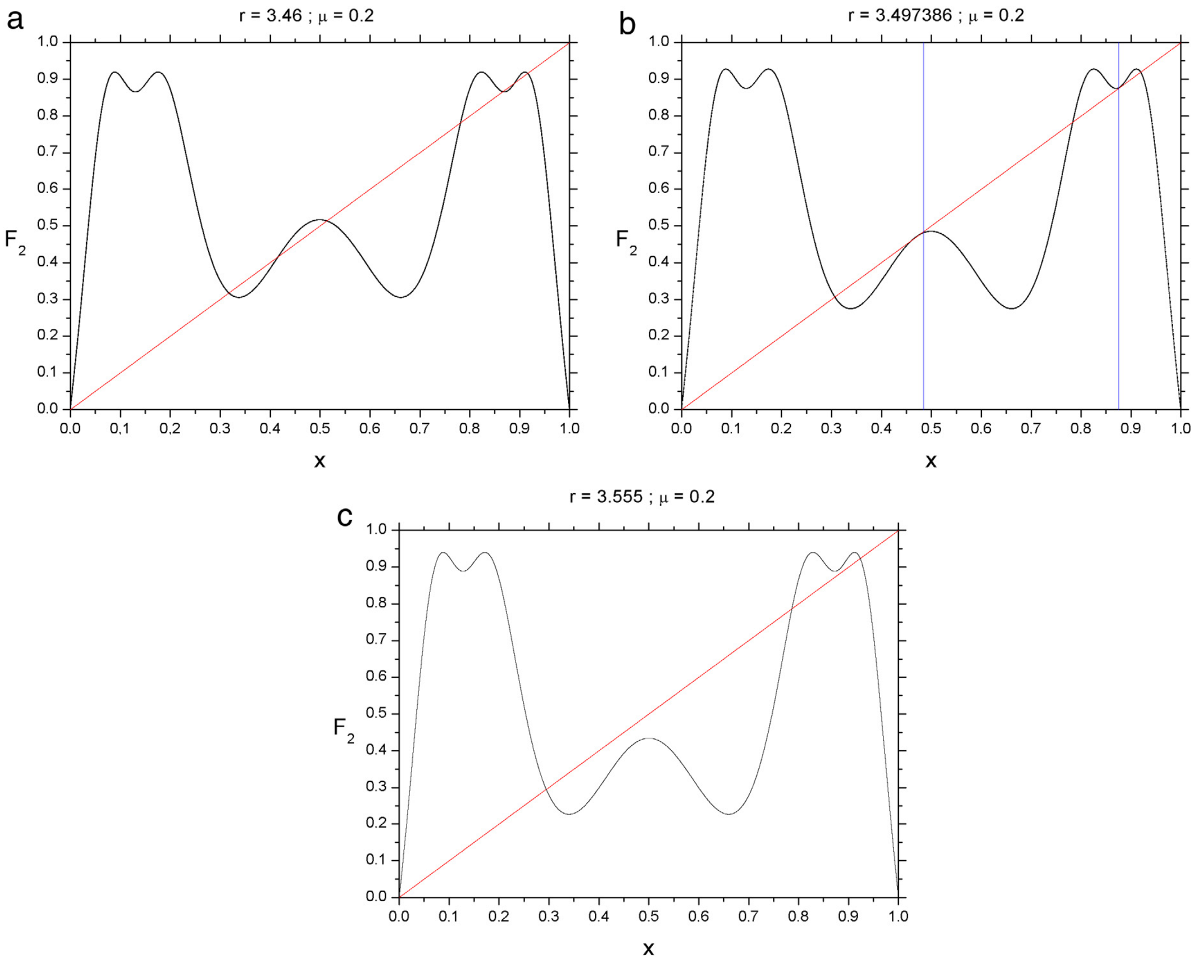

Fig. 3. Plots of the 2th composite function F_2 for (a) $r = 3.46$ before the periodic attractor finds the chaotic attractor; (b) $r = 3.497386$, when occur two near tangent bifurcations, indicated through the two vertical blue lines; (c) $r = 3.555$ far from the tangent bifurcation.

has again period-8 and for $r \sim 3.36$ occurs a second recomposition, followed by a third recomposition at $r \sim 3.42$. In the range $r \in [3.42, 3.45]$, two more branches were born and now there are two attractors, each one of period-2. We point out that we tried to go back from $r \sim 3.45$ in order to have a better understanding on these attractors but it is still not clear for us where they have started. We divided then the range $r \in [3.35, 3.45]$ in steps of size 10^{-8}. The intriguing result comes up from $r \sim 3.45$ because the period-4 attractor takes two different routes. The outer branches (blue arrows) exhibit a cascade of flip bifurcations producing two seemingly noisy cycles, while the inner ones (red arrows) do not bifurcate, do not produce noisy cycles but they touch the local chaotic attractors. These encounters do not generate crises too. Therefore what we are announcing is a collapse of a point attractor into a chaotic attractor, or a route to chaos which does not follow the flip bifurcations cascade. In Fig. 3 we observe that this collapse occurs after a tangent bifurcations of period-2, associated with one attractor of period-2 near $r = 3.497386$.

It is worth to emphasize that the well-known Gauss map [5] written as $x_{n+1} = \exp(-bx_n^2) + c$ presents similar regions of recomposition, however such recompositions occur associated with a chaotic dynamics.

In the plots of Fig. 3, we present the 2th composite function, $F_2 = f(f(x_n))$ in the range $x \in [0, 1]$ for three different values of the parameter r in order to have one more information on the collapse of the periodic attractor with the chaotic attractor. In the plot (a) we used $r = 3.46$ which shows a scenario before the collapse; in the plot (b) we chose the parameter $r = 3.497386$, which is the approximate value for the collapse, leading the function F_2 to two near tangent bifurcations, indicated through the two vertical blue lines, and the periodic attractor into the chaotic attractor; in plot (c) for $r = 3.555$, which corresponds to a chaotic region in Fig. 2, F_2 is far from the tangent bifurcation. The straight red line is the line $F_2 = x$.

In order to verify the merging region between the point and the chaotic attractors, we amplified both regions of Fig. 2 indicated by the red arrows and we show them in Fig. 4 in the range $r \in [3.49730, 3.49760]$ with steps of size 10^{-8}. Looking at the panel (a) of Fig. 4 we do not observe any flip bifurcation, but we observe a continuous sequence for the point attractor toward the chaotic attractor. In panel (b) of Fig. 4, the corresponding Lyapunov exponent is presented using the initial

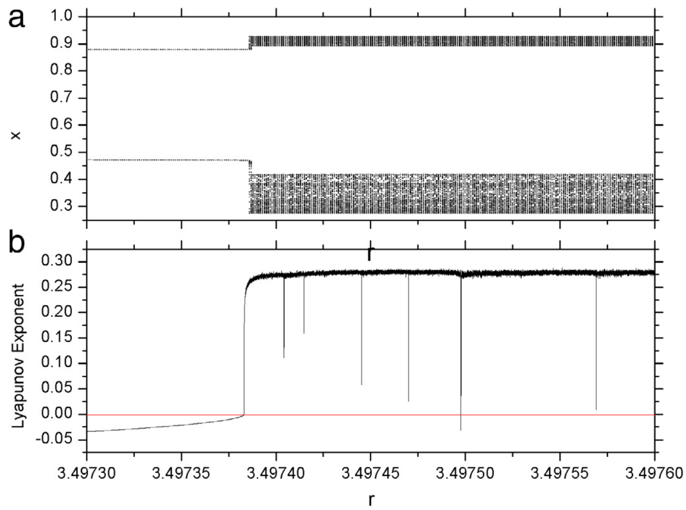

Fig. 4. Panel (a) shows an amplification of the regions of Fig. 1 (or Fig. 2) indicated by red arrows, showing a route to chaos without flip bifurcations; panel (b) shows the associated Lyapunov exponent. The red line is to guide the eye.

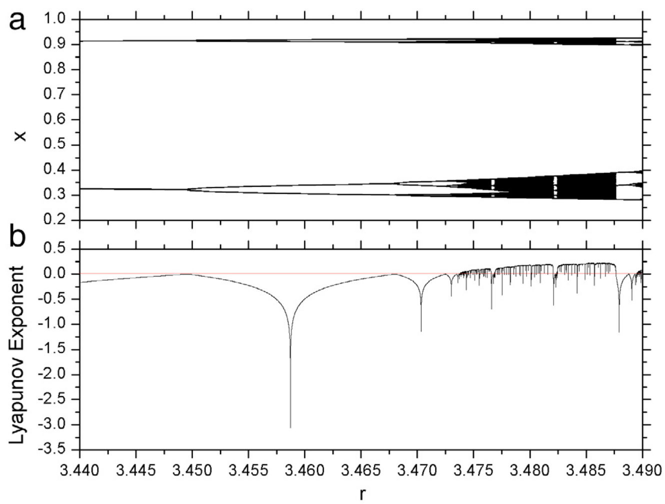

Fig. 5. In panel (a) we show an amplification of the regions of Fig. 1 (or Fig. 2) indicated by the blue arrows. This route to chaos is different of the one amplified in Fig. 4. The red line is to guide the eyes.

condition $x_0 = 0.47$. We observe a sudden transition from negative to positive around $x \sim 3.49738$ which corroborates the observation of the absence of flip bifurcations.

Analogously, in the panel (a) of Fig. 5 we amplified the merging regions indicated by the blue arrows of Fig. 1 (or Fig. 2) in the range $r \in [3.440, 3.490]$ with steps of size 10^{-6} and we observe indeed the usual cascade of flip bifurcations. In panel (b) of Fig. 5 the corresponding Lyapunov exponent was obtained from the initial condition $x_0 = 0.3$ and we observe the usual pattern of flip bifurcations of the logistic map.

Fig. 6 presents the Lyapunov diagram, which corresponds to the projections of the Lyapunov exponent in the space of the parameters r and μ. We chose the range for μ around the value we are using $\mu = 0.2$, while the range for r is the same of Fig. 2. The colors pallet shows steps of 0.1 among them. The black one indicates values for Lyapunov exponents higher than 0.3, while the light blue corresponds to values lower than -0.6. In Fig. 6(a) we have chosen the initial condition $x_0 = 0.3$, which falls in the basin of attraction of the outer attractor (the one pointed with the blue arrows in Fig. 2), while in Fig. 6(b) we started the initial condition in $x = 0.2$, which is in the basin of attraction of the inner attractor (the one pointed with the red arrows in Fig. 2). Parameters, r and μ were divided in 10^3 steps and the initial condition was iterated 10^4 times for each pair (r, μ). The red and the green line at $\mu = 0.2$ in both figures and the other two vertical red and green lines at $r \sim 3.44$ and $r \sim 3.49$ illustrate approximately both regions of collapse pointed out with the arrows in Fig. 2. We kept the same pallet of colors in both figures to become easier the comparison. Even though this range is very thin, we can observe a

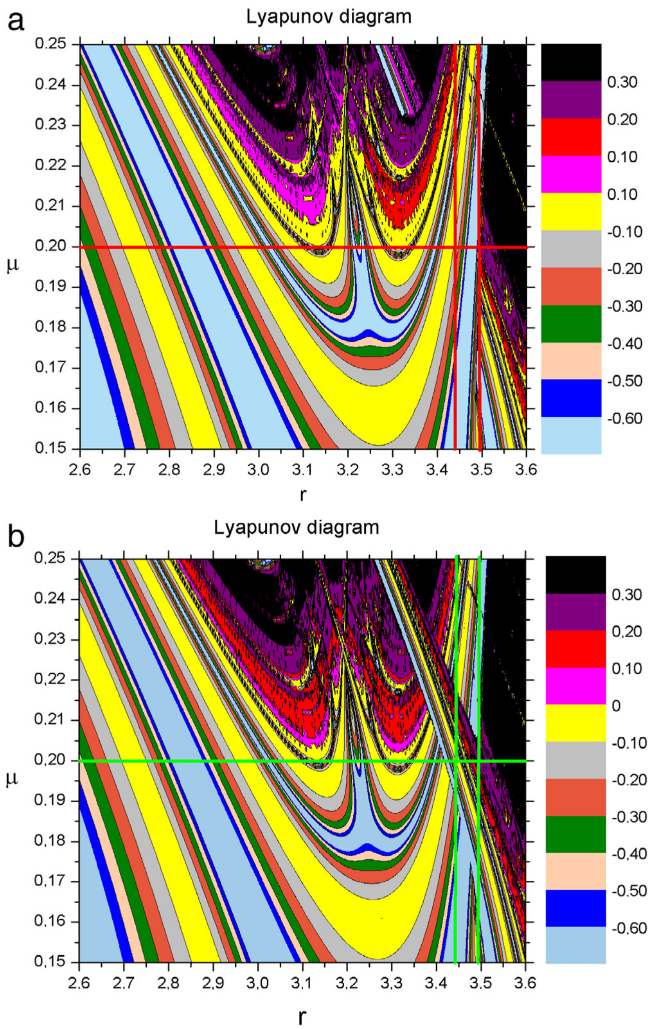

Fig. 6. Projections of the Lyapunov exponent for an initial condition started in: (a) $x_0 = 0.3$ in which we show a green line at $\mu = 0.2$ and other two vertical green lines at $x \sim 3.44$ and $x \sim 3.49$ illustrating approximately the regions pointed out in Fig. 2 with blue arrows; (b) $x_0 = 0.2$ whose red lines show approximately the regions pointed out with red arrows in Fig. 2.

subtle difference between the colors for these values of r, for $r \sim 3.44$ the Lyapunov exponent is negative (yellow), while for $r \sim 3.49$ it is positive (purple). This is in agreement with Figs. 4 and 5. The main difference between both scenarios is a long strip that is in front the main structure in Fig. 6(a), while in Fig. 6(b) this strip is behind the main structure. This difference leads to different colors and consequently different Lyapunov exponents.

In Fig. 7, we present the dynamics of the fixed points of map presented in Eq. (1). The origin is stable until the bifurcation with the other fixed point and from there it becomes unstable until $r \sim 4.0$. The r-dependent fixed point was obtained numerically from Newton–Raphson method [12] with accuracy of 10^{-10} and we divided r in steps of size 10^{-5}. For each value of r we looked for the roots of the function,

$$g(x_n) = -x_n + rx_n(1 - x_n) + \mu \sin^2(2\pi x_n), \tag{2}$$

starting with different values of x for each r. We calculated its stability by looking at the values of the first derivative of f (x_n),

$$\frac{\mathrm{d}f}{\mathrm{d}x_n} = r(1 - 2x_n) + 2\pi\mu \sin(4\pi x_n), \tag{3}$$

and by evaluating if $\left|\frac{\mathrm{d}f}{\mathrm{d}x_n}\right| < 1$ *or* > 1. When such values are smaller than 1, the fixed point is stable, hence initial conditions chosen near it converge to it as time goes on, otherwise it is unstable. The unity value would announce the eminence of stability loss. We present in blue (stable) and red (unstable) colors the corresponding stretches marking both stable and unstable regions of period-1, which come since $x \sim -\infty$ and oscillates until $x \sim 0.2$. Along this route there is

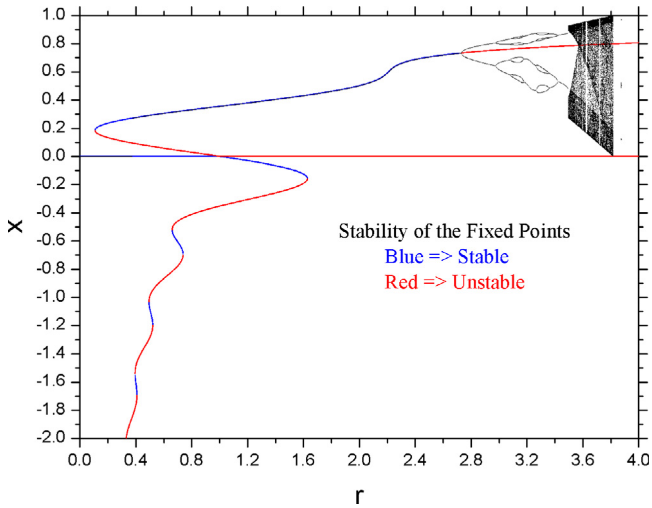

Fig. 7. Stability of the fixed points. The origin presents a transcritical bifurcation represented by the change blue–red colors. The r-dependent fixed points present a rich sequence of saddle–node bifurcations. The dynamics of the map is also presented in black. Two crises occur when the red lines touch the chaotic black regions.

a bifurcation always in the neighborhood of an extreme of the inverted function $r(x)$. In fact such oscillations indicate the existence of more than one fixed point. For instance for $r \sim 0.7$, and negative x, there are three fixed points. For $r \sim 0.9$ occurs a transcritical bifurcation with the fixed point at the origin and it becomes unstable until a next extreme at $r \sim 0.1$, from where it becomes stable up to the first flip bifurcation at $r \sim 2.73$. From this value it remains unstable until $r \sim 4.0$. For completeness we included in this plot the iterated map given by Eq. (1). For $r \sim 3.57$ this fixed point, in its unstable fashion, hits the chaotic attractor producing a crisis which merges two noisy cycles, similarly to the logistic map.

Let us now investigate the influence of the sine function for the convergence to the fixed point at the bifurcations and near them. Fig. 8(a) shows the convergence to the fixed point at $x = 0$ and $r = 1$, which marks a transcritical bifurcation. We see that for short n and depending on the initial condition x_0, the dynamics keeps the orbit confined in a constant plateau of x. Eventually, the plateau bends toward a regime of decay after reaching a critical crossover iteration number n_x. The decay is given by a power law of the type $x \propto n^{\beta}$ where β marks the speed of the decay. The crossover iteration number is clearly dependent on the initial condition with a law of the type $n_x \propto x_0^z$. The plateau scales with $x(n) \propto x_0^{\alpha}$ where $\alpha = 1$. As discussed in Ref. [13], the exponents are related among them by a scaling law of the type $z = \alpha/\beta$. At the transcritical bifurcation, the exponents obtained numerically were $\beta = -0.99994(1)$ and $z = -1.00004(1)$. Therefore the presence of the second nonlinearity in the mapping has not affected the time evolution to the stationary state nor the scaling features observed in the logistic-like model [13]. Applying a rescale in the two axis of Fig. 8(a), all curves shown in the panel (a) overlap onto each other in a single and universal plot, as can be seen in Fig. 8(b). Near the bifurcation the convergence is no longer given by a scaling function, but rather it is described by an exponential function of the type $[x(n) - x^*] \propto e^{-n/\tau}$ where τ is the relaxation time given by $\tau = (r - r_c)^{\delta}$. Here r_c defines the bifurcation parameter and the exponent δ gives the speed of the decay. The procedure to obtain δ is the following. We give an ensemble of 10^4 close initial conditions and we evolve them with the map. As soon as each orbit gets closer to the fixed point, at a distance smaller than 10^{-8}, we take the number of iterations that has spent to satisfy that condition, for each initial condition, and we perform an average of them, in such way that this average corresponds to the relaxation time τ.

By plotting τ *vs*. $(r - r_c)$, with $r > r_c$, the slope of the curve gives δ as shown in Fig. 8 for the transcritical bifurcations. Our numerical simulations furnished $\delta = -1.023(6)$ (see Fig. 9).

The next step is to move forward and investigate the convergence to the r-dependent fixed point at the bifurcation observed in the positive side of x. To do so, we need first to obtain the precise location of the bifurcation, r_c, as well as the fixed point x^*. To obtain both r_c and x^*, we notice however that two conditions have to be fulfilled simultaneously:

1. Fixed point condition: $x_{n+1} = x_n = x^*$, which leads to $g(x)$ given in Eq. (2);
2. Saddle–node bifurcation condition: the derivative of Eq. (2), Dg is evaluated at x^* and is set equal to 1, in which $Dg = -1 + r - 2rx + 2\pi\mu \sin(4\pi x)$.

These two conditions specify indeed a set of two non-linear equations that have to be solved simultaneously. The numerical method we have used is the generalized Newton's method [12] for systems of transcendental equations. We assume that an approximation $\vec{y}_k = (x_k, r_k)$, for the root (x^*, r_c), falls in a domain D where the bifurcation occurs. Then there should exist a vector $c_i \in D$, with $i = 1$ or 2 and $c_1 = x$ and $c_2 = r$, such that,

$$\vec{H}_i(\vec{y}) = \vec{H}_i(\vec{y}_k) + [\vec{\nabla} H_i(c_i)]^T (\vec{y} - \vec{y}_k), \tag{4}$$

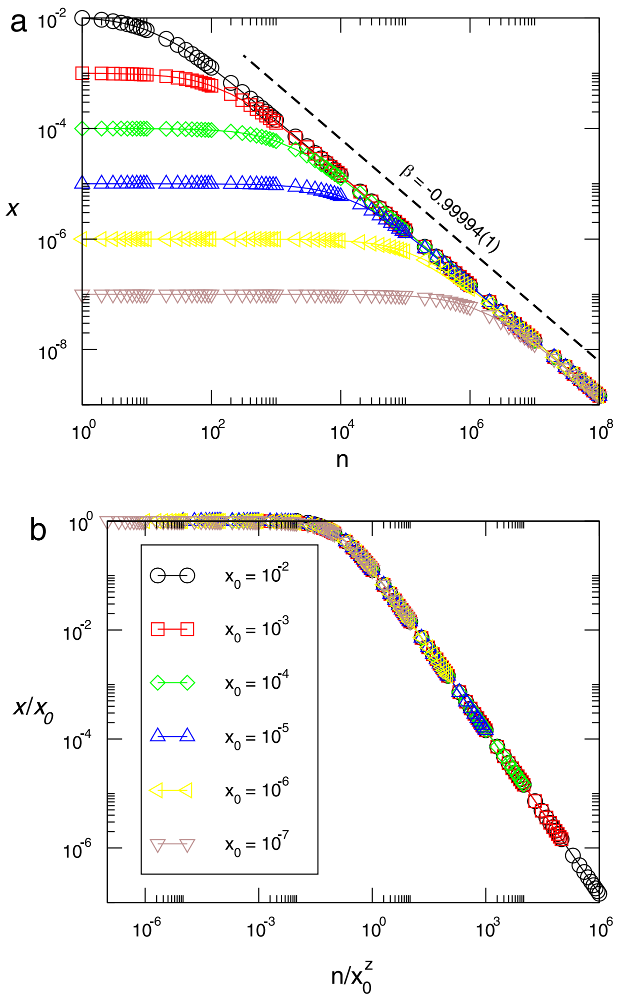

Fig. 8. In panel (a) we show the evolution of the fixed point $x^* = 0$ considering different values of x_0; in panel (b) we present the overlap of the curves, shown in (a) onto a single and universal plot after the following transformations: $x(n) \to [x(n)/x_0]$ and $n \to [n/x_0^z]$, with $z = -1$. The parameters used were $r = 1$ (transcritical bifurcation) and $\mu = 0.2$.

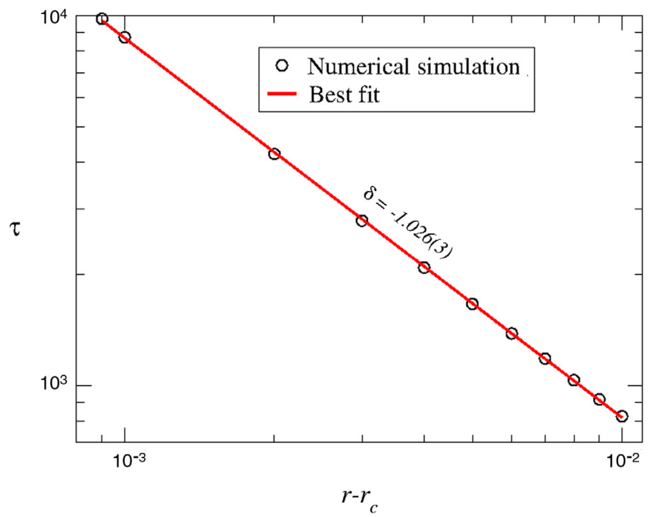

Fig. 9. Logarithm plot of τ *vs.* $(r - r_c)$, with $r < r_c$. A power law fitting gives $\delta = -1.023(6)$ for the transcritical bifurcation.

where $\vec{H} = (g(x, r),\ Dg(x, r))$ and T stands for the transposed. When the term $[\vec{\nabla} H_i(c_i)]$ is close to the term $[\vec{\nabla} H_i(\vec{y}_k)]$, Eq. (4) corresponds to a local approximation of $[\vec{H}(\vec{y})]$ around $\vec{y}_k$, hence leading to

$$\vec{H}(\vec{y}) = \vec{H}(\vec{y}_k) + J(\vec{y}_k)(\vec{y} - \vec{y}_k) \tag{5}$$

where $J(\vec{y}_k)$ is the Jacobian matrix evaluated at $\vec{y}_k$ which is written as,

$$J = \begin{pmatrix} \dfrac{\partial g}{\partial x} & \dfrac{\partial g}{\partial r} \\ \dfrac{\partial Dg}{\partial x} & \dfrac{\partial Dg}{\partial r} \end{pmatrix}. \tag{6}$$

An approximation for the root is obtained when $\vec{H}(\vec{y}) = \vec{0}$, leading to

$$J(\vec{y}_k)\vec{S}_k = -\vec{H}(\vec{y}_k) \tag{7}$$

where $\vec{S}_k = (\vec{y} - \vec{y}_k)$ is the solution of Eq. (5). Then, from an initial approximation $\vec{y}_k$ a next iteration is $\vec{y}_{k+1} = \vec{y}_k + \vec{S}_k$. The procedure is repeated as many times as necessary until the accuracy criterion $|x_{k+1} - x_k| \leq 10^{-14}$ is attended, and $|r_{k+1} - r_k| \leq 10^{-14}$. With these requirements, we obtained the coordinates of the bifurcation in the positive side of x at $r_c = 0.10966817250056$, which produces a fixed point $x^* = 0.18364048565559$. So, since r_c and x^* are known, then the exponents α, β, z and δ can be obtained numerically. The first exponent is $\alpha = 1$. The decay is marked by the exponent $\beta = -0.982(2)$, while $z = -1.018(2)$. The last exponent is $\delta \approx -1$.

The same procedure used for such bifurcation can be extended to the period-doubling bifurcation taking into account that the flip condition is marked by (Dg), evaluate at x^*, equal to -1. Under this condition as well as the condition $x_{n+1} = x_n = x^*$, the first period doubling bifurcation is observed at $r_c = 2.73178612223300$, yielding a fixed point to be observed at $x^* = 0.73268422374886$ both represented with an accuracy of 10^{-14}. The exponents obtained numerically marking the convergence to the fixed point are $\alpha = 1$, $\beta = -0.49937(5)$, $z = -2.0025(2)$ and $\delta \approx -1$. The typical convergence to the fixed point for both bifurcations is well illustrated by Fig. 8.

3. Conclusions

As short summary, in this work we present the collapse of a point attractor into a chaotic attractor through a route which is preceded by a tangent bifurcation, different of the usual bifurcation cascade followed by the second periodic attractor. The qualitative differences between both attractors are pointed out especially in the plots of Fig. 6. We also report an alternating sequence of changes of stability of the r-dependent fixed points between stable and unstable. It is worth to emphasize that this multiple stability changes took us by surprise, because it was not expected and it is not still clear for us what is the responsible mechanism which produces the fixed point's birth and such saddle–node bifurcations. Surely, it deserves further studies. However, the introduction of the second nonlinearity to the mapping did not affect the convergence to the fixed points near and near at the bifurcations. The scaling laws discussed in Ref. [13] are also valid for the mapping discussed here.

Acknowledgments

We acknowledge support from the Brazilian scientific agencies FAPESP-São Paulo Research Foundation through the grants 2014/00334-9 and 2012/23688-5; CNPQ-National Council of Technological and Scientific Development through the grants 306034/2015-8 and 303707/2015-1; CAPES-Coordination for the Improvement of Higher Education Personnel and FUNDUNESP-Unesp Development Foundation.

References

[1] R.L. Devaney, A First Course In Chaotic Dynamical Systems: Theory and Experiment (Studies in Nonlinearity), Westview Press, 1992.
[2] R.M. May, Science 86 (1974) 645.
[3] C. Grebogi, E. Ott, J.A. Yorke, Phys. Rev. Lett. 48 (1982) 1507.
[4] C. Grebogi, E. Ott, J.A. Yorke, Physica D 7 (1983) 181.
[5] R.C. Hilborn, Chaos and Nonlinear Dynamics: An Introduction for Scientists and Engineers, Oxford University Press, New York, 1994.
[6] J.A.C. Gallas, Phys. Rev. Lett. 70 (1983) 2714.
[7] P. Collet, J.-P. Eckmann, Iterated Maps on the Interval as Dynamical Systems, Birkhauser, Boston, MA, 1980.
[8] M.J. Feigenbaum, J. Stat. Phys. 21 (1979) 669.
[9] M.J. Feigenbaum, J. Stat. Phys. 19 (1978) 25.
[10] P.D. Beale, Phys. Rev. A 40 (1989) 1.
[11] E.D. Leonel, R. Egydio de Carvalho, Phys. Lett. A 364 (2007) 475.
[12] J.D. Hoffman, S. Frankel, Numerical Methods for Engineers and Scientists, second ed., Marcel Dekker Inc., New York, 2001.
[13] R.M.N. Teixeira, D.S. Rando, F.C. Geraldo, R.N. Costa Filho, J.A. de Oliveira, E.D. Leonel, Phys. Lett. A 379 (2015) 1246.